Underwater Object Tracking Using Electrical Impedance Tomography

James Snyder[1], Yonatan Silverman[2], Yang Bai[2] and Malcolm A. MacIver[1,2,3]

Abstract— **Few effective technologies exist for sensing in dark or murky underwater situations. For this reason, we have been exploring the use of a novel biologically-inspired approach to non-visual sensing based on the detection of perturbations to a self generated electric field. This is used by many species of neotropical nocturnal freshwater fish. This approach, termed active electrosense, presents unique challenges for sensing and tracking of nearby objects. We explore two methods for estimating the velocity of objects through active electrosense. The first of these methods uses a simple cross-correlation method, which depends on the uniformity of the electric field. We show some of the ramifications of making this assumption for a self-generated field around a cylindrical pod-shaped sensor in a rectangular tank. We then evaluate the use of methods developed for electrical impedance tomography (EIT) for localization and tracking. This is an unusual application of EIT in that typical applications involve surrounding the volume of interest (such as the thorax of humans) with sensor/emitters. Here, rather than this "outside in" approach, we are using EIT "inside out." In simulation, we nonetheless find significant improvements in the accuracy of estimated velocity when using the EIT approach. Additionally, we demonstrate how EIT may be used for accurate position estimation. Under the conditions evaluated, the computation time for inversion is low enough to make its use feasible as a primary position and velocity estimator in an on- line system or as a secondary system to augment a computationally inexpensive estimator.**

I. Introduction

Weakly electric fish make use of a self-generated weakly electric field to navigate, hunt, and communicate with other conspecifics in their environment. The animal emits a weak oscillating electric field and senses perturbations in this field with an array of electroreceptors distributed over the surface of the skin. These perturbations are induced by objects whose conductivities differ from the surrounding fluid. Studies of this sensory modality, termed active electrosense, in these animals during hunting behavior reveals an ability to detect very small objects (3 mm long aquatic prey) on the order of $1/3$ the animal's body length in distance [1].

This ability to track prey or other objects as they come within range of the field would be of great utility in translating electrosense to an underwater vehicle context. With this sense the robotic platform could estimate its relative velocity and position with respect to objects within its environment. This would be useful both for navigation and interaction with objects in the environment.

One important consideration when translating a sensory modality of this type into robotic contexts is understanding how field magnitude and orientation comes about. The field structure derives from the geometry and impedance of the emitting body and other objects or boundaries in the environment.

Just as there exists perspective distortion with wide-angle lenses, the field structure and its drop-off with distance leads to a form of spatial distortion in measurable voltages [2]. In order to interpret position or other properties of objects, these distortions must be taken into account. With a lens and light rays, by knowing how the lens distorts light for a given focal length, one can apply distortion corrections for that configuration regardless of the scene being photographed. In contrast, for the diffusion of electrical currents into the environment, we are unable to simply put a lens in front of the sensor and adjust focal length. Instead, the body that is emitting the field, the environment nearby the emitter, and the nearby objects are all components of a complex lens.

The diffusion effect coupled with the interaction with the environment yields a severely ill-posed inverse problem for relating measurements to the surrounding environment, requiring *a priori* knowledge about environmental boundary conditions and geometry in order to limit the solution space for the inverse problem. The use of of this *a priori* knowledge coupled with regularized regression approaches is called Electrical Impedance Tomography (EIT) [3], [4]. This methodology employs the use of an array of transceiver electrodes spread along the boundary of a conductive medium, where pairs of electrodes are alternately used to source and sink current and to measure the resulting voltages in the space. By doing this one is alternately setting and measuring boundary conditions. This technique has been applied for medical and geophysical applications where imaging of the impedance of a space provides diagnostic utility [5], [6], [7], [8].

In this paper, we consider estimation of object position and velocity with an EIT-based method and velocity alone with a simpler cross-correlation method which assumes a uniform field structure. The cross-correlation method is appealing due to limited computational complexity, but performance is degraded in non-uniform electric fields, where non-uniformity is a function both of the emission source and environment geometry. The EIT-based method requires greater computational complexity, but provides conductivity estimates for the full 3-D volume being observed, therefore providing position

*This work was supported by NSF grants IOB-0517683 and CMMI-0941674 to M.A.M., and an Office of Naval Research Small Business Technology Transfer grant N00014-09-M-0306 to M.A.M.

[1]Department of Biomedical Engineering, R.R. McCormick School of Engineering and Applied Science, Northwestern University, Evanston, Illinois, United States of America

[2]Department of Mechanical Engineering, R.R. McCormick School of Engineering and Applied Science, Northwestern University, Evanston, Illinois, United States of America

[3]Department of Neurobiology, Northwestern University, Evanston, Illinois, United States of America

information in addition to velocity. In both cases, we use the geometry of a cylindrical pod, termed the sensorPod, with a pair of electrodes at either end of the major axis, and pairs of electrodes positioned with equal separation along the lateral, top and bottom surfaces (Fig. 2) placed within a confined tank environment. The tank dimensions are chosen, in part, because the sensory range for our electrolocation objects is on the order of the largest distance between the current emitting electrodes. The near-field sensing characteristic of active electrosense makes it well suited to sensing within confined spaces or near substrates such as the ocean floor [9].

In our cross-correlation computational experiment, we show the performance of a configuration where only the electrodes at the ends of the long axis of the sensorPod are used for sourcing and sinking current, and a set of lateral differential voltage measuring pairs are used to estimate velocity using a simple cross-correlation algorithm. This approach works by attempting to determine the lag between signals "seen" on neighboring pairs of differential sensors as the sensorPod moves by the object within a confined space (for practical purposes we usually move the object by a fixed sensorPod to the same effect). We then compare this with the performance of an EIT-based system, in simulation, using the same geometry to estimate position and velocity of an object moving by the pod at varying lateral distances.

II. Methods

A. Velocity using cross-correlation

The uniform field example was computed by setting field magnitude to a constant value on a grid of points. Voltages at the electrodes were then computed using an induced dipole method [2]. Electrodes were positioned at x=$\pm$ 0.035 m, z=0, y=$\{0,\pm$ 0.0254, $\pm$0.0508$\}$. For the self- generated field example, a 3-D mesh was created using Gmsh [10] for

a 0.75 $\times$ 0.75 $\times$ 0.2 m tank ($x,y \approx 4\times$ the pod length in y) with an insulating cylindrical pod at the center (Fig. 2). Faces for the electrodes at either end of the model were fixed at $+1$ V and -1 V respectively (Dirichlet boundary conditions), and the potential at each cell in the mesh was computed using FiPy [11] according to continuum Kirchoff's law, where free charge density (current sources) has been set to zero:

$$\nabla \cdot \sigma \nabla \phi = 0$$

where ϕ is the electric potential and σ is the conductivity. Conductive objects were added to the scene by selecting the cells within a circular region of a given radius and adjusting the conductivity coefficient to a value 10 mS while the surrounding fluid was set to 200 μS. Voltages for this field were interpolated to the lateral electrode positions on the surface of the pod matching the geometry of those in the uniform field.

In both cases, an object was moved through space with x fixed for each trial in a range of +0.05 to 0.28, z was fixed at 0, and y was varied from -0.35 to +0.35 m, so that the object passed by the pod at a fixed x (lateral) distance from near one extreme in the y direction to the other (Fig. 1).

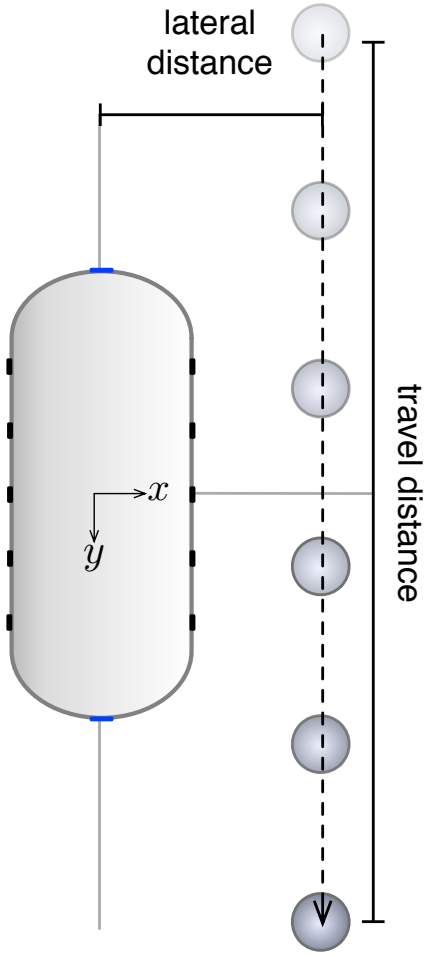

Fig. 1. **Configuration of Object Pass** This figure illustrates the general configuration of the object passes. $x,y,z = 0$ at the pod center. Lateral distance is the object x position. y is maximum at start and end of travel distance, all trials are symmetrical about the x axis.

Voltages on opposite sides of the pod were subtracted to remove the common mode of the field and enable high differential gain. These voltages were then cross-correlated as neighboring pairs to find the temporal delay between a feature appearing on one pair and the next, and the separation of electrodes (2.54 cm) was used to then relate the cross-correlation and the temporal profile of correlation between voltage pairs to estimate velocity.

B. Inversion Using EIT

The same geometry description and mesher [10] used for the self-generated non-uniform field example above was used to generate new meshes. A medium resolution 3-D mesh was used to simulate the forward solution and low resolution mesh was used for reconstruction of conductivity using EIDORS (electrical impedance and diffuse optical tomography reconstruction software) [12].

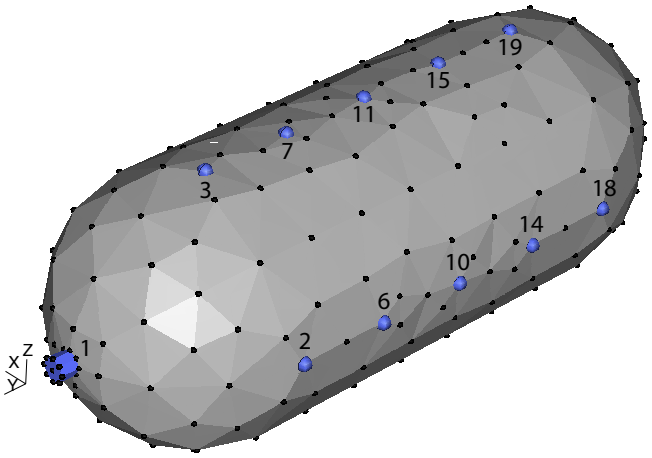

Fig. 2. **Meshed surface of the sensorPod** Blue cylinder in bottom left and blue spheres show electrodes. A second cylindrical electrode is present but not visible behind the body in the top right (forming the primary and y axis, $x, y, z = 0$ at the center of the pod geometry). One set of lateral electrodes and top electrodes are visible. An additional set is present on the other side, mirrored about the $y-z$ plane. Electrodes on the bottom mirror the top set about the $x-y$ plane. Black points illustrate vertex points. Pod length in y is 0.19 m (including cylindrical electrodes), diameter (and separation between lateral electrodes) is 0.07 m

Electrodes along the sides of the pod were duplicated and placed on the top and bottom to bring the total count to 22 electrodes (Fig. 2). The mesh resolutions were selected in order to enable a ~ 5 second cycle time for computing forward and inverse reconstructions on an 8-core Intel Xeon machine.

Objects were simulated moving past this geometry at varying fixed distances, matching the protocol used for the cross-correlation velocity estimation simulations (Fig. 1). At each object position, instead of fixing the two major-axis cylindrical electrodes at voltages and measuring differential lateral pairs of electrodes, electrodes were modeled as transceivers capable of sourcing or sinking fixed current levels while voltages were measured at other sensor pairs. Numbering of electrodes started at one end-cap electrode and spiraled down the major axis of the pod (Fig. 2). Stimulation patterns were selected in a rotating fashion such that the first and sixth electrode were initial current source/sink and that voltages were measured between the remaining pairs with the same separation (first 2nd and 7th then 3rd and 8th, etc..).

Reconstructions were performed using a built-in one-step regularized Gauss-Newton reconstruction [13] method with a Laplace prior, and a hyperparameter (λ) selected for the noise conditions of the trial [4]. For cases where noise was not added, $\lambda = 0.1$ was used. For the -80 dB noise case, $\lambda = 50$ was used. Solutions yielded conductivity estimations for all the elements in the mesh.

The resulting estimates of the conductivity in all regions of space around the sensorPod were then thresholded such that elements below 91% of the maximum computed conductivity were set to zero. The positions of the nodes for the remaining elements were then used as estimations of object position (mean x, y & z) and uncertainty (using the difference between the 10% and 90% quantiles).

C. Kalman filter

The position and uncertainty values derived from the suprathreshold element positions were then used as measurements (z_k) and associated independent components of noise (R) in a Kalman filter. The control input model (B) and control model (u_k) are implemented for velocity control with velocity derived from the derivative of prescribed object positions and independent process noise (Q) was fixed at 1 mm.

III. Results

A. Cross-correlation

Estimation of velocity using cross-correlation of differential electrode voltages yields accurate final velocity estimates at distances up to 0.17 m from the center of the tank (Fig. 3). At greater distances, velocity is overestimated as signals become more diffuse and voltage differences do not settle fully to zero at the beginning and end of the trajectory.

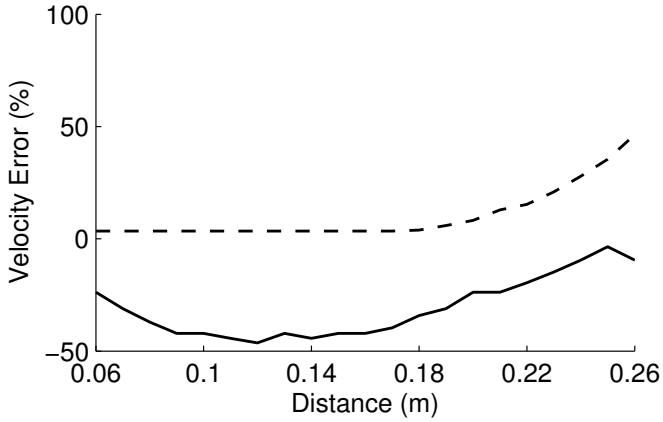

Fig. 3. **Velocity Estimation Using Cross-correlation** Percent velocity error with varying lateral distance for a uniform field (dashed) and a self-generated field (solid). Self-generated field error is least near the pod and outer edge of the tank. Uniform field error increases at greater distances as image becomes more diffuse and object travel distance is not long enough for accurate estimates.

When the same method is applied to a self generated field whose structure is influenced by the shape of the insulating pod and the tank where the pod resides, estimates begin with -23% error at 0.06 m, dip to a maximum error of -46% at 0.12 m and then recover to approximately -3% error at a distance of 0.25 m.

B. EIT with Kalman filter position & velocity

Using EIT for 3-D reconstructions of conductivity with thresholding yielded higher accuracy and precision during periods where the object was closest to the pod (y positions between -0.15 and 0.15) (Figs 4, 5). x position errors for

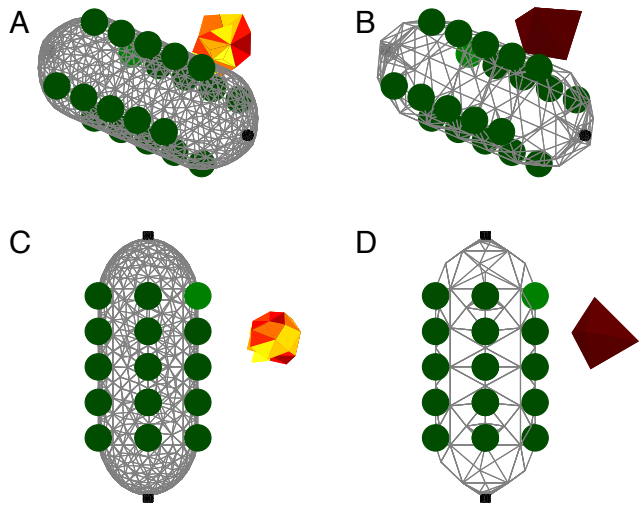

Fig. 4. **Forward and Inverse Conductivity** Left plots (A,C) show two views of the conductivites prescribed onto elements of the mesh to be used in computing the forward solution. Right views (B,D) show thresholded reconstructions on a low-resolution mesh. 3-D object position is accurately estimated when near the pod (lateral distance is 0.09 m). $\lambda = 0.1$

a 0.09 m distance pass were less than 0.1 m for peak conductivity position and 0.025 m for the Kalman filter estimates. Mean error for the filtered data was higher than the average peak position at -0.012 m. Similar maximum error performance is seen for y position, with mean error for the filtered data at 0.003 m. Error magnitude of differences between actual and estimated positions shows similar differences for peak error, however the mean magnitude position error for the Kalman filter is $\sim 1/2$ that of the peak element position estimates.

When varying distances are considered, the magnitude error estimate is lowest near the pod, increasing to a distance of 0.2 m, then dropping as the object gets closer to the edge of the tank. Error for the filtered position estimates is lower at all distances.

When velocity is derived from this position data (Fig. 7) and percent error is computed, the maximum error for the Kalman filter is $1/6$ the peak element-based estimates at a distance of 0.09 m. Mean error for the kalman filter is 4% compared with 10% for unfiltered data. When velocity estimates were evaluated at varying distances (Fig. 8, Table I), the filtered error is approximately half that of the unfiltered data throughout the range. When compared with self-generated field cross-correlation estimates, error for the kalman filtered data is $1/10$ the cross-correlation estimate at a distance of 0.12 m, with the difference decreasing until the cross-correlative estimate shows a lower velocity error at a distance of 0.24 m.

Adding -80 dB (relative to emission voltage magnitude) of noise to voltage measurements for both cross-correlation and EIT methods yields significant increase of variance with distance (Fig. 9, Table I). Kalman filter and cross-correlation estimates begin with similar magnitude error (18% vs 19%)

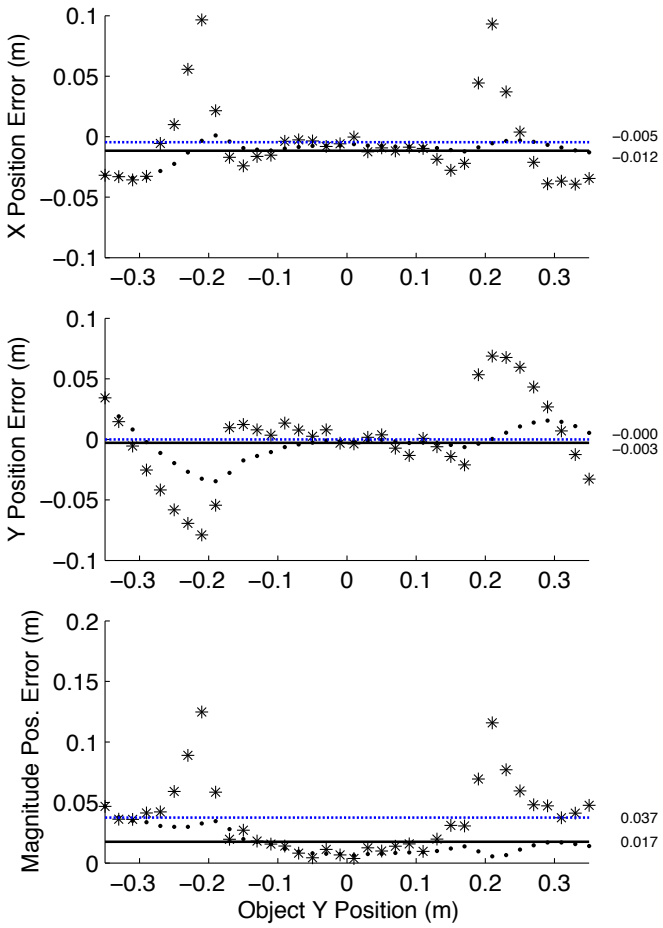

Fig. 5. **Position Estimation using Kalman Filter** Per-position X, Y, and error magnitude for peak conductivity element (stars), Kalman filter (dots) and mean errors for peak conductivity element (blue, dotted) and Kalman filter (black). Kalman filter position estimates show significantly lower error for all comparisons. Lateral distance from center fixed at 0.09 m). $\lambda = 0.1$

at 0.06 m, but at greater distances the Kalman filtered results remain more consistent up to 0.14 m, where error and variance increase greatly for the cross-correlation method.

IV. Discussion

A. Cross-correlation

Velocity estimation with cross-correlation provides accurate velocity estimates up to a distance of $\sim 1/4$ the length of the trajectory traversed (Fig. 3), at which point the bipolar curve representing a single sensor's view of the object becomes wide enough that voltages no longer settle to 0 for each sensor at the completion of the trajectory. As a consequence, the cross-correlation algorithm makes increasingly large errors in determining the lag between signals and overestimates velocity.

In a non-uniform self-generated field, the velocity estimate varies as a function of distance as the field structure changes yielding increasing then decreasing error quantities as field structure is most uniform near the pod and at the edge of the tank.

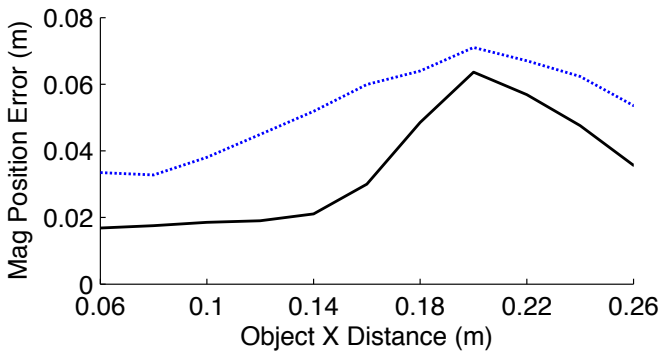

Fig. 6. **Mean Position Error at Varying Distances** Mean magnitude of position error for passes at varying lateral distances from the major axis of the pod. The blue dotted line represents peak element-based velocities, the black line shows Kalman filtered data. Filtered data performs better all distances tested, greatest ratio of improvement between distance of 0.08 and 0.16 m. $\lambda = 0.1$

	0.06	0.10	0.14	0.18	0.22	0.26
CC	-23%	-42%	-44%	-34%	-19%	-10%
EIT (pk elem.)	-8%	-9%	-10%	-13%	-17%	-20%
EIT (Kalman)	-4%	-4%	-4%	-7%	-9%	-12%
CC (-80 *dB*)	-19%	-37%	-79%	-119%	-105%	-90%
IQR	2%	13%	138%	76%	83%	156%
EIT (Kal.-80 *dB*)	18%	17%	16%	-35%	-42%	-72%
IQR	3%	3%	2%	59%	53%	16%

TABLE I

PERCENT ERROR FOR MEAN VELOCITY ESTIMATES AT VARYING DISTANCES (IN METERS) FOR CROSS-CORRELATION (CC) AND EIT. FOR -80 *dB* CASES HAVE -80 *dB* OF NOISE ADDED AND VALUES ARE MEDIANS FOR $N = 20$, THE INTERQUARTILE RANGE (IQR) FOR BOTH -80 *dB* CASES IS SHOWN ON THE LINE BELOW THE MEDIANS.

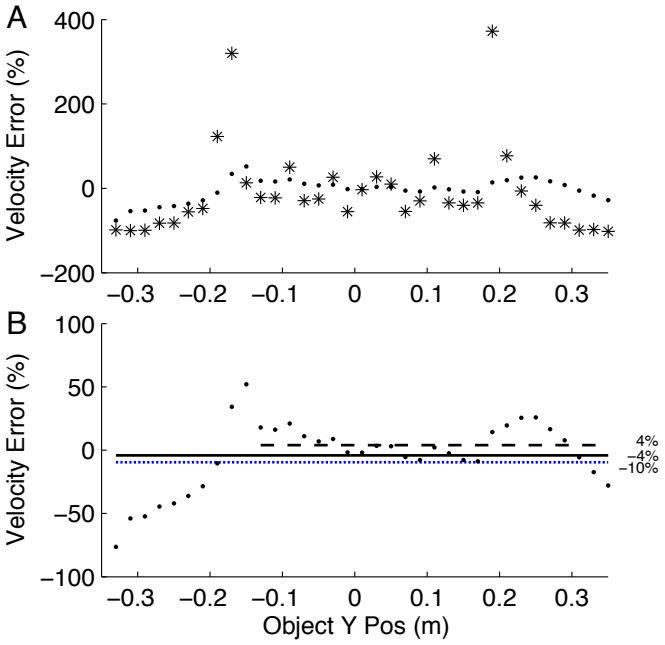

Fig. 7. **Velocity Estimation using Kalman Filter** A) Velocity error for peak element position (stars) and Kalman filter estimate (dots). B) Kalman filter velocity error (dots), average peak element error (blue, dotted), average Kalman filter error (black) and last 2/3 trial Kalman filter error (dashed). Lateral distance from center fixed at 0.09 m. Kalman filter reduces overall velocity estimation error and minimizes the responses to jumps in position of the peak-element data.$\lambda = 0.1$

B. Kalman filter position & velocity

By using measurement techniques and algorithms developed for electrical impedance tomography, we were able to localize an object in a simulated conductive media. By using an adaptive threshold to only consider the highest conductivity portion of the reconstructed space, we were able to track the movement of that object and use the spread of above-threshold conductive elements as an uncertainty estimate for a Kalman filter. Peak position errors for x & y components remained below 2.5 cm for a pass at a distance of 9 cm from the primary axis of the sensorPod. As distance was increased, the magnitude of position error increased for both filtered and unfiltered cases, reaching a peak at 0.2 m (Fig. 6). This peak point shows a tendency for estimates to be increasingly biased towards the outer edge of the tank as distance is increased. Once this distance is reached, above-threshold elements make contact with the boundary wall of the volume for every step. A similar phenomenon can be observed during each object pass, where the position error reaches a maximum around 0.2 m in the Y direction (Fig. 5).

When velocity error is compared between the filtered EIT measurements and previous cross-correlation data for a self-generated field, the filtered EIT configuration performs significantly better through most of the distance ranges evaluated, with a maximum reduction of an order of magnitude in error at a distance of 0.12 m (Fig. 8). At increasing distances this performance gap reduces, however, based on prior experimentation with a pod of similar geometry in an actual tank where the signal to noise ratio was approximately -80 *dB* (relative to emission magnitude), and performing similar simulations (Fig. 9, Table I), error for velocity estimation is lower and more consistent for the EIT-based method.

C. Computational Complexity

The use of regularized regression techniques from EIT is a much more computationally intensive task than the cross-correlation method. This scales in memory and computation time with increasing numbers of mesh elements. In particular, computation of the Jacobian matrix and regularization can take up the bulk of the time from a cold start to the ability to perform a first inversion on a mesh [14]. For the configuration used in this paper, these computations can take 1-2 minutes. However, when the same mesh is used for multiple steps, using a cached Jacobian matrix and regularization matrix allow for cycle times for subsequent solutions of ~ 5 seconds (including forward solution and plotting) on an 8-core 2.40 GHz Xeon machine with memory usage below 2 GB. Time for the inversion step represents < 30 ms of that time.

The startup computation costs for the more expensive parts of the solution can be reduced by pre-computing the

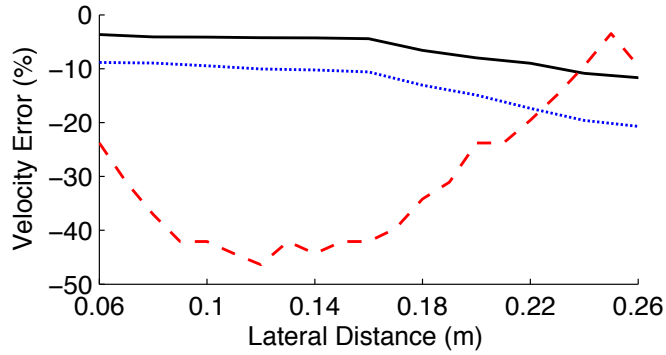

Fig. 8. **Mean Velocity Error at Varying Distances** Mean velocity error fo r peak element (blue, dotted), Kalman filtered data (black), cross-correlation with self-generated field (red, dashed). This figure shows velocity error performance at varying lateral distances from the pod, estimates are averages for trials at lateral distance. Kalman filtered data performs significantly better than cross-correlation data until a distance of 0.22 m. $\lambda = 0.1$ for EIT

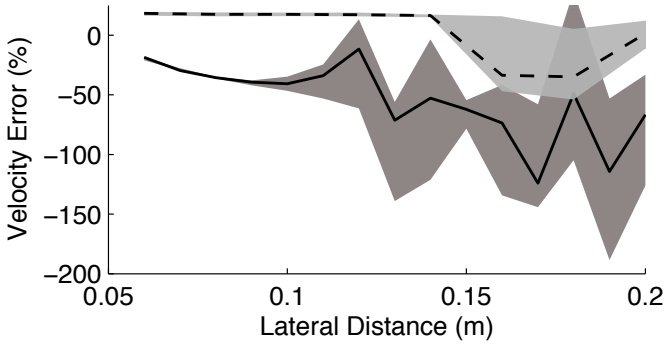

Fig. 9. **Mean Velocity Error at Varying Distances with** -80 *dB* **noise** Mean velocity error for kalman filtered data (dashed line, with interquartile range (IQR) shaded light grey, $n = 20$, for each distance), cross-correlation velocity estimate (solid line, IQR shaded dark grey, $n = 20$ for each distance) with $-80-dB$ of noise added. This figure shows velocity error performance at varying lateral distances from the pod, estimates are averages for trials at lateral distance. Cross-correlation estimate becomes more variable at lateral distances greater than 0.1 m. Filtered EIT approach provides more consistent estimates up to 0.14 m. $\lambda = 50$ for EIT

Jacobian and regularization matrices for a set of meshes representing different environmental conditions. Under such conditions, depending on the required update rate, an EIT-based method could be used alone with relatively low cycle times, or in conjunction with other estimators like cross-correlation which would require corrections based on object position in order to provide consistent tracking. Additionally, the EIT community is exploring methods for reducing the computational costs of computing these steps by use of other algorithms [14].

V. Conclusion

In order to accurately estimate position and velocity of objects in a space using a self-generated electric field, it is necessary to integrate *a priori* knowledge about the geometry of the space in order to correct for variations in the field structure of a self-generated field. When used alone, without knowledge of the environment or variations in field structure, methods such as cross-correlation of lateral differential voltages yield variable amounts of error dependent on object distance. If the relative geometry of the space is known, our simulations suggest that methods developed for medical and geophysical imaging can be used for position and velocity estimation of objects moving relative to a submersible sensor platform. These estimates could be used alone or in conjunction with other less computationally intensive techniques to provide continuous velocity and position estimates.

In addition, these techniques can be used more broadly on this type of platform (without thresholding or the Kalman filter) to image the impedance in environments where other sensory apparatus such as vision would not be usable or provide as much information about the space around the sensory platform.

References

[1] M. a. MacIver, N. M. Sharabash, and M. E. Nelson, "Prey-capture behavior in gymnotid electric fish: Motion analysis and effects of water conductivity," *J. Exp. Biol.*, vol. 204, no. 3, pp. 543–557, Feb. 2001. [Online]. Available:

[2] B. Rasnow, "The effects of simple objects on the electric field of Apteronotus," *Journal of Comparative Physiology A*, vol. 178, no. 3, pp. 397–411, Mar. 1996. [Online]. Available:

[3] A. P. Calder and A. P. Calderón, "On an inverse boundary value problem," in *Seminar on Numerical Analysis and its Applications to Continuum Physics*, W. H. Meyer and M. A. Raupp, Eds., vol. 25. Rio de Janeiro: Soc. Brasileira de Matemàtica, 1980, pp. 65–73.

[4] W. Lionheart, N. Polydorides, and A. Borsic, "The reconstruction problem," in *Electrical Impedance Tomography*, ser. Series in Medical Physics and Biomedical Engineering, D. Holder, Ed. Taylor & Francis, Dec. 2004, vol. 20041231, ch. 1. [Online]. Available:

[5] I. Frerichs, "Electrical impedance tomography (EIT) in applications related to lung and ventilation: a review of experimental and clinical activities," *Physiological measurement*, vol. 1, 2000. [Online]. Available:

[6] B. H. Brown, "Electrical impedance tomography (EIT): a review." *Journal of medical engineering & technology*, vol. 27, no. 3, pp. 97–108, 2003. [Online]. Available:

[7] A. Kemna, B. Kulessa, and H. Vereecken, "Imaging and characterisation of subsurface solute transport using electrical resistivity tomography (ERT) and equivalent transport models," *Journal of Hydrology*, vol. 267, no. 3-4, pp. 125–146, 2002. [Online]. Available:

[8] D. LaBrecque, A. Ramirez, W. Daily, A. Binley, and S. Schima, "ERT monitoring of environmental remediation processes," *Measurement Science and Technology*, vol. 7, p. 375, 1996. [Online]. Available:

[9] M. E. Nelson and M. A. MacIver, "Sensory acquisition in active sensing systems," *Journal of Comparative Physiology {A}: Neuroethology Sensory Neural and Behavioral Physiology*, vol. 192, no. 6, pp. 573–586, 2006.

[10] C. Geuzaine and J. Remacle, "Gmsh: A 3-D finite element mesh generator with built-in pre-and post-processing facilities," *International Journal for Numerical Methods in Engineering*, vol. 79, no. 11, pp. 1309–1331, Sept. 2009. [Online]. Available:

[11] J. E. Guyer, D. Wheeler, and J. A. Warren, "FiPy: Partial Differential Equations with Python," *Computing in Science & Engineering*, vol. 11, no. 3, pp. 6–15, May 2009. [Online]. Available:

[12] A. Adler and W. R. B. Lionheart, "Uses and abuses of EIDORS: an extensible software base for EIT." *Physiological measurement*, vol. 27, no. 5, pp. S25–42, May 2006. [Online]. Available:

[13] A. Adler and R. Guardo, "Electrical impedance tomography: regularized imaging and contrast detection." *IEEE transactions on medical imaging*, vol. 15, no. 2, pp. 170–9, Jan. 1996. [Online]. Available:

[14] A. Boyle, A. Adler, and A. Borsic, "Scaling the EIT Problem," in *12th Conf. Electrical Impedance Tomography*, no. May, Bath, UK, 2011.